eprints@whiterose.ac.uk
https://eprints.whiterose.ac.uk/

A Systematic Approach to Climate Resilience Assessment of Infrastructure Networks

Qianqian Li, Giuliano Punzo, Craig Robson, Hadi Arbabi, Martin Mayfield

Abstract—With a changing climate, the frequency and intensity of extreme weather events are likely to increase, posing a threat to infrastructure systems' resilience. The response of infrastructure systems to localized failures depends on whether assets are affected randomly, in a targeted strategic way, or in any way in between. More than that, infrastructure decisions today, including new routes or improvements to existing assets, will underpin the behavior of the systems over the next century. It is important to separate and analyze the case of climate-based disruptions and how they affect systems' resilience. This paper presents a probabilistic resilience assessment framework where failure scenarios and network disruptions are generated using weather profile data from climate prediction models with component-level fragility functions. A case study is then carried out to quantify the resilience of Great Britain's railway passenger transport system to high-temperature-related track buckling under the Representative Concentration Pathway 8.5 (RCP8.5) climate change scenario. A 95-year horizon on the resilience of the railway system is drawn. The results reveal the non-linear responses of the railway system to the increasing temperature and show that models considering random asset failures overestimate the system's resilience.

Index Terms—Network resilience, infrastructure networks, climate change

I. Introduction

A. Background

The centrality of infrastructure systems in society, and therefore their resilience to disruptions in a complex, fast-evolving environment, are now universally recognized [1], [2]. Extreme weather events such as storms and floods can extensively affect the functionality and serviceability of infrastructure systems [3]–[5]. The current climate change trajectory is only likely to result in an increased frequency and intensity of such events [6], [7]. Although current infrastructure systems have been stressed by various types of events from time to time, they are generally considered to be resilient to specific natural hazards as they are designed, built, and operated in compliance with design codes and regulations set on historical meteorological data [8]. Yet, design standards and operational standards, and therefore the system's capacity to absorb shocks, are defined over expected magnitudes of shocks. Such expectations have been largely surpassed by the scale of extreme weather events caused by climate change [9]–[11]. Therefore, current infrastructure systems may not have the ability to withstand the future climate, characterized by more frequent and intense weather extremes. What is resilient to the present-day climate may be vulnerable to the future climate. An understanding of how weather hazards impact infrastructure systems is required.

Since the publication of the Intergovernmental Panel on Climate Change (IPPC) Fifth Assessment Report [6] and the open access to climate model output data, there has been an increasing body of literature on assessing the impacts of climate change on infrastructure systems. For example, the third Climate Change Risk Assessment [12] assesses the future flood risk to Great Britain and estimates the number of assets exposed by overlapping the flood risk maps with the geographical maps of the assets and identifying those likely to surpass specific indices or risk thresholds. Other impact assessments appearing in the literature have been carried out in a similar manner. They rely on estimating the likelihood of surpassing certain design or operational thresholds under several climate change scenarios [13]–[15].

For the classification and determination of the impact of climate hazards, a two-tier approach is proposed in [16], where the approach first distinguishes direct and indirect impact. Direct impacts refer to consequences related to the infrastructure system itself, including complete or partial damage to physical infrastructure assets, deviation of performance from the fully functional level, and connectivity loss. Indirect impacts refer to those received by the society that is served by the infrastructure systems, such as causalities, community isolation (both physical and in terms of communications), and economic losses. By this classification, the majority of existing climate change impact assessments, including [12]–[15], are on the physical damage level.

Under the scope of climate change impact assessments, functional damages are rarely analyzed, often just viewed as a consequence. Works related to functional damage and system-level loss of service, in particular, are comparatively more limited in number [17], [18]. Limiting impact assessments to the estimation of physical damages or even component-level functional loss overlooks the complex interdependencies of infrastructure systems [1]. Infrastructure systems are well acknowledged as complex coupled systems, the behavior or response of which is distinct from the combined behavior or response of its components [19]. Impact assessments on physical damage level certainly provide valuable insights into the magnitude of climate-change-related disruptions. However, the complex dynamics characterizing infrastructure systems' responses are such that system-level effects cannot be derived in a straightforward manner from the component level. Therefore, an understanding of how more extreme weather events,

including those not normally seen in geographic areas in the past, may cause a hazard and impact infrastructure systems is required.

B. State of the Art

Existing works on system-level responses to disruptive events are often cast within research in resilience, as well as the related areas of vulnerability and robustness. A resilience assessment often starts with modeling real-world infrastructure systems as networks. Network models in literature can be categorized into two groups: topological models and flow models. In a topological model, e.g., [20], [21], physical infrastructure system assets, such as rail stations, transmission lines, and airports, are modeled as nodes or edges in the network. These models emphasize the topological structure of the system but lack the ability to capture the functional aspect of the infrastructure system: where the demands are, where the supplies are, and how any demand can be met. A flow model, e.g., [22], has its emphasis on the services and flows delivered by the infrastructure system more than the network's topological structure. Flow models are normally expressed as OD (origin-destination) matrices. In a flow model, nodes are entities that either supply, demand, or transit services or goods. Edges capture flows between pairs of nodes. Recent works on system-of-systems, interdependent, or interconnected networks adopt a combined topological and flow model (e.g. [23]–[25]). Such models have separated asset and flow layers representing the physical infrastructure assets as a graph and the services provided, respectively. Inter-layer dependencies describe the physical embedding of a service end-node into the asset layer, that is, in which asset node a flow between two nodes of the flow layer is originated or delivered by means of the physical network of assets.

Disruptions are mostly simulated as strategic removals of network components [26]. This type of network component removal is often referred to as an *attack* in abstract network studies [27]. The most common strategies used for network attacks are either random, where nodes and edges are randomly selected and removed from the network, or targeted, where nodes and edges are selected based on their structural/topological importance in the network [26]. The random attack strategy resembles some real-world disruption events like random equipment failure, operational faults, and accidents [23]. The targeted attack strategy, to some extent, aims at capturing events like malicious attacks [28] or some theoretic worst-case scenarios. While random disruptions and targeted attacks are useful simplifications, they do not completely cover the wide variety of possibilities that a real-world scenario may present. Many disruptive events, particularly weather-related events, may not fit into either.

Although weather events feature stochasticity, they are not purely random because the climate has deterministic dynamics that exhibit chaotic behaviors [29]. However, weather-related disruptions certainly do not maliciously target any specific network components, making the targeted attack strategy unrealistically severe. Those approaches are not capable of capturing the feature of weather-related disruptions. Furthermore,

complex networks behave differently under different attack scenarios [30]. Even if the infrastructure network of interest is shown to be resilient to random or targeted network attack strategies, it is not necessarily resilient to climate or extreme weather event-based disruptions. Therefore, the resilience of infrastructure systems to weather-related events should be simulated with realistic weather profiles in addition to random and targeted strategies.

There exist extensive works in the literature on the resilience of infrastructure systems to extreme weather events (e.g., [31]–[39]). The events are represented in various forms. For example, in [31], the weather condition across the power distribution system is characterized by two variables, the number of thunders and the maximum wind gust speed. Here we are more interested in works that use weather profiles to initiate network disruptions and in particular, works that address the spatial profiles and patterns of weather events in their assessments instead of using one single homogeneous weather condition across the entire network. A common strategy is to divide the system under study into weather regions, within which the weather conditions are assumed to be homogeneous (e.g., [34], [35].

Panteli and Mancarella [36] propose a conceptual framework to assess the influence of climate change on weather-related power interruption. In their work, an explicit reference is made to the use of weather profile data in both time and space domains to initiate system component failure and simulate cascading effects. However, subsequent works [37], [38] appear not to implement such a strategy fully. The hourly wind profiles in [37] are obtained by sampling three normal probability distribution functions representing normal, high, and extreme weather conditions. In [38], the space-varying aspect is reached by dividing the network into six weather regions. Within each region, the weather conditions are assumed to be homogeneous and are sampled with a weather simulator. Works that account for actual spatial weather patterns, e.g., [39], do so by reproducing historical wind extremes with spatial correlation. This implies the assumption that historical or present-day weather statistics will hold in the future, which is now widely recognized as a fallacy due to the changing climate and weather patterns [6], [7].

An important gap in current resilience assessment frameworks, in relation to the effects of climate change on infrastructure systems, is that weather-induced failure scenarios are simulated with manipulations of present-day weather statistics [39], [40]. What is resilient to the current patterns may easily be fragile to the future ones. Future weather profiles produced by climate models are the only viable option to assess the resilience of infrastructure systems to future extreme weather events, moving beyond the widespread extremes of random and targeted attacks, unable to capture the features and threats of climate change. An approach to simulate failure scenarios through future weather profiles generated by climate models is hence needed and proposed here.

C. Main Contributions of the Work

This paper proposes a systemic approach to assess the resilience of infrastructure systems to climate change. In doing

so, it proposes a novel quantitative framework that returns the statistical distribution of the system's response as produced by weather profile data for the relevant geographical area. These are obtained from climate model outputs and projected onto the geographical asset location of an infrastructure system. Moving beyond the current approaches to quantify infrastructure network resilience, this work:

- proposes a method to initiate network disruption based on local climate hazards obtained from weather profiles/data with a 95-year horizon;
- assesses system-level functional loss based on the service level retained, which considers possible reconfiguration, as opposed to a mere count of the failed nodes or the identification of a threshold for network fragmentation;
- brings the physical damage and service loss quantification together to return a measurement of the infrastructure systems' resilience to extreme weather events-based failure scenarios;
- benchmarks the method through a case study on Great Britain's railway network, including disruptions to the ability to satisfy the travel demand.

The proceeding sections are organized as follows. Section II describes key components in the resilience assessment framework, offering a clear account of the formulation proposed, which can be replicated for further research or adapted to specific infrastructure systems. In Section III, the proposed framework is applied to Great Britain's railway network with high-temperature-related failures. Discussion and conclusions are offered in Section IV and Section V.

II. The Resilience Assessment Framework

The proposed method uses standard weather profiles obtained from the Earth System Grid Federation [41], which holds the most extensive collection of observational, reanalysis, and simulation data for climate change research. Those weather profiles are available as individual time series of weather parameters, such as wind, precipitation, and humidity, with different time resolutions and geographical ranges. The key elements of the proposed approach, namely the network model, the failure scenario generation, and the probabilistic resilience measure are described in more detail later in this section. It is worth mentioning that resilience in this work does consider the recovery stage, where rerouting and repairing activities are concerned, but the recovery algorithm is not detailed in this section as they could be interchangeable depending on the case study or the infrastructure sector being analyzed. The high-level architecture of the proposed framework is shown in Figure 1.

A. Network Representation of Infrastructure Systems

In this work, the infrastructure system is modeled as a bi-layer network, constituting an asset and a flow layer. The reason for this is twofold. Provided the ultimate purpose of an infrastructure system is to provide a service or services, a resilience measurement that relates to the system's ability to maintain the delivery of services when exposed to external

For a weather event $E_{\mathcal{T}}$ defined by time stamp $\mathcal{T}$:
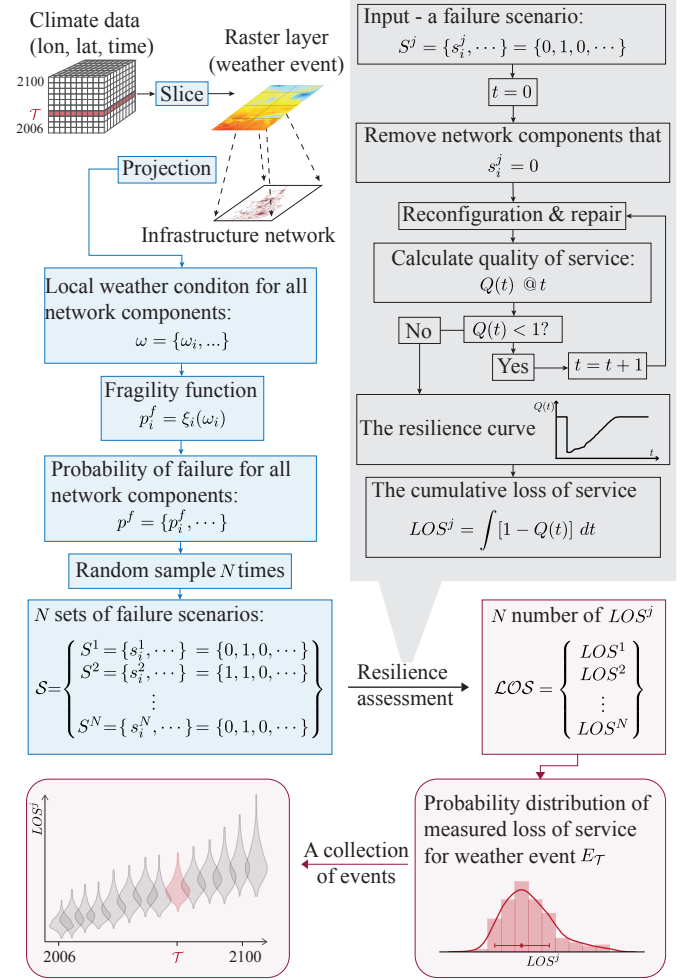

Fig. 1: Overview of the probabilistic resilience assessment framework. Failure scenarios are sampled with weather profiles across the network. Service disruption is then calculated for each sampled failure scenario, forming a probability distribution. The resilience of infrastructure systems to future climate is assessed with a collection of such probability distributions.

shocks would be better than one relating to the extent of damage/change on its topological structure. The second reason is that such separation makes it possible to incorporate multiple asset layers and, therefore, multiple types of climate hazards into the assessment. The successful delivery of a unit of service can sometimes rely on multiple interdependent infrastructure systems with components in each system affected by different types of climatic hazards. The separation makes it possible to initiate failures in different asset layers caused by different climate hazards simultaneously while increasing the flexibility of the modeling framework to adapt to different infrastructure systems.

In the following, the asset and flow layers will be indicated by subscripts α and ϕ, respectively. Hence, for the asset layer, assets can be thought as a graph $\mathcal{G}_\alpha = \{\mathcal{V}_\alpha, \mathcal{E}_\alpha\}$ where $\mathcal{V}_\alpha$ and $\mathcal{E}_\alpha$ indicate the set of nodes and edges, respectively. The

framework does not need to differentiate node assets and edge assets rigidly. For layer α, $\mathcal{A}$ indicates the set of assets in layer α, with elements $\mathcal{A}_i$, $i = 1, 2, \cdots, .|\mathcal{V}_\alpha| + |\mathcal{E}_\alpha|$, with $|\cdot|$ indicating the cardinality of a set. The equivalent definitions for the flow layer ϕ are omitted for brevity.

B. Failure Scenario Generation

In this work, a *failure scenario* refers to a set consisting of the simultaneous failure and removal of network components. The generation of such failure scenarios follows a systematic approach using the obtained climate model output (the blue boxes in Figure 1). The climate outputs are three-dimensional (3D) data, where spatial weather data are combined with the third dimension of time. A *weather event* refers to a slice from the 3D data with a desired geographical range and timescale. For a given weather event, by projecting the weather data on the asset layer, the local weather condition for all network components in the asset layer can be found.

$$\omega = \{\omega_i, ...\}, \ i = 1, 2, ...|\mathcal{V}_\alpha| + |\mathcal{E}_\alpha|$$

where ω_i is the local weather condition for asset $\mathcal{A}_i$.

With the local weather condition allocated for each asset network component, a non-zero asset failure probability arises as the asset may fail due to local weather conditions. This probability defines the likelihood that an asset can withstand an assigned local weather condition and can be derived from a fragility function, which returns the probability of failure as a function of the magnitude of the local weather conditions. Such fragility function can be obtained by gathering relevant information from the asset management company where available. The shape of a fragility curve reflects uncertainty in the asset's ability to withstand a shock. If the failure is deterministic (e.g., a circuit breaker in an electric circuit triggered by a given value of the current), the fragility function takes the shape of a step function with a threshold (Figure 2a), beyond which the probability of failure passes abruptly from 0 to 1. Examples used in the literature are air temperature threshold for railway track buckling [15] and significant wave height on port operation [42]. The threshold model, or step function, assumes that asset failures are deterministic when the assigned shock is above the threshold. When there are greater uncertainties in the asset's capacity to withstand a shock, a more general sigmoid function can be used (Figure 2b). Examples of the latter include [37]–[39], where sigmoidal fragility functions are associated with the failure of electricity transmission lines and towers to local wind speed.

In the most general form, consider the fragility function for each network component in the asset layer as

$$p_i^f = \xi_i(\omega_i), \tag{1}$$

where ξ_i stands for the fragility function for asset $\mathcal{A}_i$ and p_i^f is the calculated probability of failure for asset $\mathcal{A}_i$ when the local weather condition is ω_i. The probability of failure for all network components in the asset layer is

$$p^f = \{p_i^f, \cdots\}, \ i = 1, 2, ...|\mathcal{V}_\alpha| + |\mathcal{E}_\alpha|.$$

For the sake of simplicity, and without loss of generality, all assets are assumed to have a binary state. The state of a single
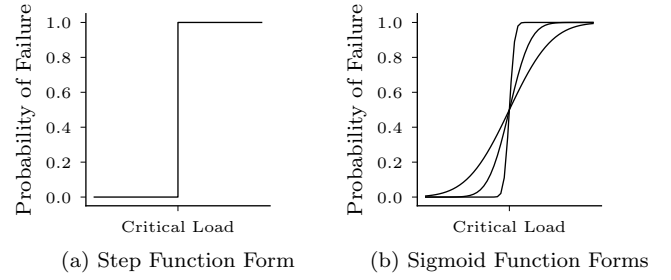

(a) Step Function Form　　(b) Sigmoid Function Forms

Fig. 2: Example fragility curves.

network component, $\mathcal{A}_i$, can therefore be described by an independent Bernoulli random variable $X_i \sim Ber(p_i^f)$ that:

$$P(X_i) = \begin{cases} p_i^f, & \text{for } X_i = 0 \\ 1 - p_i^f, & \text{for } X_i = 1 \end{cases}. \tag{2}$$

The state of the whole network is therefore effectively controlled by a set of independent Bernoulli random variables

$$\mathcal{X} = \{X_i, \cdots\}, \ i = 1, 2, ...|\mathcal{V}_\alpha| + |\mathcal{E}_\alpha|,$$

where each X_i corresponding to some failure probability.

One sample of each random variable returns a failure scenario for the system, where network component failures are initiated by removing assets with $X_i = 0$. Each failure scenario represents one possible outcome from the weather event. The complete sample space for $\mathcal{X}$ is of size $2^{|\mathcal{V}_\alpha| + |\mathcal{E}_\alpha|}$. To reduce the complexity of simulating the system's response to all $2^{|\mathcal{V}_\alpha| + |\mathcal{E}_\alpha|}$ combinations, a Monte Carlo approach is used to estimate the possible outcomes. Through repeated sampling, N set of possible failure scenarios can be obtained with

$$\mathcal{S} = \{S^j, \cdots\}, \ j = 0, \cdots, N,$$

where j denotes a single Monte Carlo run. Each subset, S^j, contains a combination of states for all network components and is regarded as a single failure scenario.

C. Probabilistic resilience measure

The UK National Infrastructure Commission (NIC) lists 'anticipate, resist, absorb, adapt and transform' as key aspects of infrastructure resilience [43]. While 'robustness, resourcefulness, rapid recovery, adaptability' are identified as the four main features of resilience by the National Infrastructure Advisory Council of the USA [44]. Such definitions of resilience include the recovery stage and consider not only the system's ability to maintain its service at the time of event happening but also its ability to maintain service between event-happening to the time of full recovery. This paper considers resilience as the ability of a system to maintain and return to its normal operations after a disruption occurs. Here the resilience metric proposed by Bruneau et al. [45] is adopted for its general applicability and inclusion of the recovery stage. Resilience, R, is measured as cumulative service degradation from the time of the earthquake, or any disruptive events,

happening, t_0, to the time of full recovery, t_1, as shown in Equation (3):

$$R = \int_{t_0}^{t_1} [100\% - Q(t)] \, dt, \qquad (3)$$

where $Q(t)$ denotes the quality of infrastructure at time t in percentage, with $Q(t) = 100\%$ meaning fully functional status.

In this work, the resilience metric from [45] is modified in two aspects. First, instead of the quality of the infrastructure assets, $Q(t)$ here measures the quality of service provided. Moreover, such a measure of the quality of services may take different meanings depending on the nature of the infrastructure system under study. As a general case, it is expressed as the percentage of satisfied demand

$$Q(t) = \frac{\sum_\phi F^t}{\sum_\phi D^t}, \qquad (4)$$

where F^t and D^t denote the delivery and demand at time t respectively. The resilience metric is then calculated as cumulative loss of service

$$LOS = \int_{t_0}^{t_1} 1 - \left(\frac{\sum_\phi F^t}{\sum_\phi D^t} \right) dt. \qquad (5)$$

Second, to take the uncertainty of the system behavior into account, resilience to a given weather event is associated with the averaged LOS from all sampled failure scenarios (the red boxes in Figure 1). For a given weather event, a set of N failure scenarios, $\mathcal{S} = \{S^j, \cdots\}$, $j = 0, \cdots, N$, are randomly sampled. For each failure scenario, S^j, component failures are initiated in the asset layer accordingly, and disruptions in the service layer are then computed. Depending on the system's dynamics, reconfiguration and repair activities can then be performed. $Q(t)$, is calculated at every time step until full service is recovered. The cumulative loss of service, LOS_j, from the j-th sampled failure scenario, S^j, is then calculated with Equation 5. The statistical distribution of set, $\mathcal{LOS} = \{LOS_j\}$, $j = 0, \cdots, N$, describes the system's resilience to the given weather event.

III. Case Study - Great Britain's Railway system

Heat-related track buckling is one of the most common reasons for delays and cancellations in railway services. The UK experienced a brief but unprecedented extreme heatwave from 16 to 19 July 2022, where rail services were severely disrupted [11]. Recognizing the urgency and consequence of this issue, this section presents a case study on Great Britain's railway passenger transport system, which is modeled as a flow network dependent on a single asset layer of train tracks subjected to high-temperature related track buckling. A set of temperature projections covering the years 2006-2100 under the Representative Concentration Pathway 8.5 (RCP8.5) climate change scenario is used to generate plausible climate-based failure scenarios. Those failure scenarios are then used to initiate failures in the network, followed by the proposed resilience assessment.
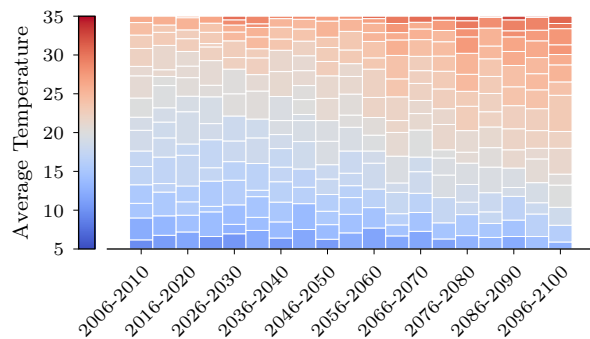

Fig. 3: Clustering of the summer days (01 May to 30 September) from 2006 to 2100 based on the tasmax of CORDEX output data EUR-11_CNRM-CERFACS-CNRM-CM5_rcp85_r1i1p1_MOHC-HadREM3-GA7-05_v2. 15 clusters are produced for each 5-year group through a K-means algorithm. The height of each bar is controlled by the number of days that fall into the cluster. The color of the bar is controlled by the average temperature of the synthetic centroid of the cluster.

A day-by-day resilience assessment for the 95-year period would hardly meet practical considerations and require substantial computational power. Summer days (May to September) in each 5-year period are clustered together using a K-means algorithm where the optimal number of clusters (K) is obtained via an elbow analysis, returning results between 8 and 15 clusters. Practically, this is done using a Bisecting K-means algorithm, coded in the Python Scikit-learn package [46], where all other parameters are set to their default values. The day closest to the synthetic centroid of each cluster is chosen as the representative day. By doing so, 285 example days are selected, representing 285 typical weather events and, thus, 285 unique distributions of climate hazards over the railway network. This approach makes the dataset computationally tractable with the method presented without losing significant information, and the 5-year interval is consistent with the size of the EURO-CORDEX data batches.

A. Model Inputs and Assumptions

In this case study, a few simplifications and assumptions are made for the balance of generality and specificity. In the absence of reliable information and empirical data, those choices are the most general and possible form. We have made our data and scripts publicly available as IEEE DataPort dataset (DOI 10.21227/d0z6-q125).

1) The network: The railway network model developed by Pant et al. [23] is used in this case study. It has separated flow and asset layers (Figure 4). The asset layer is an undirected weighted network that consists of 4024 stations, modeled as nodes; and 4524 railway track segments, modeled as edges. The flow layer is in the form of OD trips, representing the services provided. There are 2,282,270 OD pairs between 2484 origin and destination nodes out of the 4524 nodes in the asst layer. Each OD pair has an original edge path assigned, $\mathbb{P}^0_{od}$,
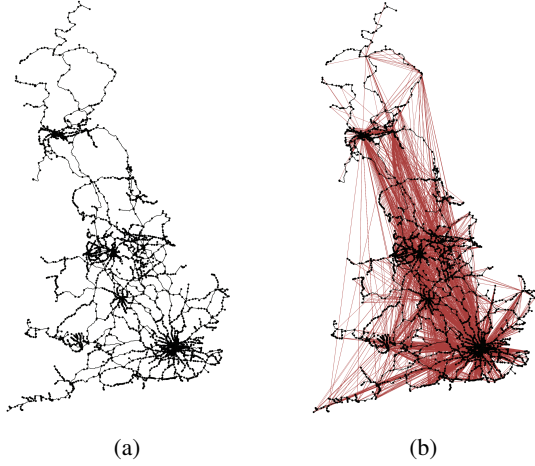
Fig. 4: (a) Asset layer of the network model with 4024 nodes and 4524 edges. (b) Flow layer of the network model. This figure only plots 22,326 out of the total 2,282,270 OD pairs, which has more than 15 passenger trips and geographical path length greater than 30km.

detailing which edges in the asset layer are utilized. Average daily traffic over the year is used as both a measure of the traffic volume on edges in the asset layer and OD demand. The system is assumed to be in a steady state with this daily traffic with the same amount of services demanded every day, regardless of the state of the asset layer. Any daily, weekly, or seasonal variations are not considered in this case study. A time resolution of one day is used.

2) The Hazard: High-temperature-related track buckling is used as an example hazard to demonstrate how to generate network failure scenarios using weather profiles. From [47], [48], track buckling is related to the daily maximum temperature. To the best of found knowledge, there is no existing fragility function that expresses the probability of track buckling as a function of the ambient temperature. The empirical definition of such a function is beyond the scope of this paper. A Gaussian sigmoid is hence considered as a fragility function with its shape controlled by the two parameters μ and σ. The fragile function, ξ_i, for asset $\mathcal{A}_i$, therefore expresses as

$$p_i^f = \xi_i(\omega_i) = \frac{1}{2}[1 + \text{erf}(\frac{\omega_i - \mu_i}{\sigma_i \sqrt{2}})], \tag{6}$$

which is controlled by 2 parameters σ_i and μ_i. μ_i is related to the Critical Rail Temperature (CRT), which is dependent on other factors such as the stress-free temperature of the rail and the degree of consolidation of the ballast [49], and σ_i is related to the confidence/uncertainty of the estimated of CRT.

The critical air temperature for heat-related track buckling varies depending on track conditions. However, track conditions are not available from the network model or network-wide from other sources. For the purpose of this case study, the dependence of the critical air temperature on track conditions is therefore not considered, and all edges in the network are subjected to the same fragility function regardless of any variations in condition. Taking the thresholds in [47], [50] into consideration, the cumulative distribution function

of $\mathcal{N}(35, 2.5)$ is used. The value of μ and σ can be tuned if more information becomes available, e.g., a collection of historical failure events and corresponding local temperature. Therefore, in this case study, the fragility function for all edges is

$$p_i^f = \xi(\omega_i) = \frac{1}{2}[1 + \text{erf}(\frac{\omega_i - \mu}{\sigma \sqrt{2}})]. \tag{7}$$

3) The Climate Data: As mentioned above, track buckling is related to the daily maximum temperature. Therefore the output variable, daily maximum near-surface air temperature (*tasmax*)), is used in this case study. EURO-CORDEX provides climate change data for the European domain, covering a period of 95 years, from 2006 to 2100. By limiting the results to:

- "domain" = "EUR-11" (0.11°, ∼12km spatial resolution),
- "experiment" = "RCP8.5",
- "time frequency" = "day",
- "variables" = "tasmax",

64 sets of model output are left. They differ in the global climate model used for downscaling, the climate model ensemble, and the regional climate model used.[1]

4) Rerouting Algorithm: Railways usually are not delivering at their maximum capacity [51]. When the network is partially damaged with some OD pairs losing their original path, the spare capacity allows rerouting to utilize the remaining assets to attempt to deliver those interrupted OD flows. When the original path is interrupted due to one or more edge failures, passengers are assumed to stay at the origin node and no passenger is waiting at any intermediate nodes on the original path. A modified minimum-cost maximum-flow algorithm based on the Edmonds-Karp algorithm [52] is used for the flow assignment here. More details about the rerouting strategy can be found in the associated IEEE DataPort dataset (DOI 10.21227/d0z6-q125).

5) Recovery: Asset repairing activities are assumed to take place at every time step until the asset layer is fully recovered. For the sake of this example and to bypass the scarcity of information on the recovery of incidents in the railway sector, damaged edges are subject to the same recovery probability of 0.5 at every time step until fully recovered. Once an asset is recovered, no secondary damage is considered in this disruptive event.

B. Simulation

As the temporal resolution for the acquired climate variable *tasmax* is daily, a single day is regarded as a weather event, which is assumed uncorrelated to conditions of the previous and following days. For a single day, the weather condition across the country is seen as an instance of situations the railway system might face. This case study considers continuous hot days or heatwaves that last longer than 24h as a single extreme event with repair work only happening after the event. This is consistent with Network Rail's operational standards,

for which track maintenance works should not be carried out when the rail temperatures are above 32 °C (corresponding to an air temperature of 21 °C) or are predicted to exceed 38 °C (corresponding to an air temperature of 25 °C) within three days of work conducted [53]. For each weather event, the local conditions for each edge are first assigned and transferred to the probability of failure using the fragility function. Then 250 sets of failure scenarios are generated through random sampling.

For the j-th failure scenario, disruptions are initiated through the removal of edges for which $s_i^j = 0$ $i = 1, 2, ... |\mathcal{V}_\alpha| + |\mathcal{E}_\alpha|$ at time step zero. Interrupted OD pairs, whose original path $\mathbb{P}_{od}^0$ includes any removed edges, are then identified. The rerouting algorithm then calculates the amount of OD flows rerouted. The total amount of delivery at this time step is the sum of the rerouted and the uninterrupted OD trips. The quality of service, $Q(t)$, is calculated with Equation 4. Undelivered OD flows, partially or completely, at the current time step, plus the steady-state daily demand (the annual average daily traffic) becomes the demand for the next time step. Asset repair is carried out between time steps until all edges are recovered. If the original path of an OD pair is recovered at a time step, from the next time step, any accumulated undelivered trips will be delivered via their original path with the 50% spare capacity fully utilized instead of rerouting.

To compare the climate-based failure scenarios to random and targeted, shocks of the same intensity should be applied to the network in two separate settings with either a random or targeted strategy. This 'intensity' is taken as the number of edges removed in this work. For a given day, the expected number of failed edges can be calculated as

$$\Psi = E(\mathcal{X}) = \sum_{i=1}^{|\mathcal{E}_\alpha|} E(X_i) = \sum_{i=1}^{|\mathcal{E}_\alpha|} p_i^f. \qquad (8)$$

This implies that if a weather event was set as a random attack on the network assets, on average, Ψ edges would be randomly selected and removed in each Monte Carlo run. For the targeted strategy, edges with the most traffic are removed first. In both cases, the same resilience assessment procedure as in the climate-based failure scenarios is followed.

Using Python, the simulations are carried out by Intel Xeon E5-2630 v3 CPUs. Each example day with a given failure strategy (climate-based, random, or targeted) is submitted as a batch job. Each batch job is allocated 16G of RAM. The CPU time for the 285 example days with climate-based failure scenarios is 1792 hours in total. The CPU time for random and targeted strategies is 1904 hours and 1881 hours, respectively.

C. The 95-year trend

For any given failure scenario, with the resilience defined as in Section III, the quality of service drops immediately upon the removal of edges. With rerouting and repairing efforts, the quality of service gradually bounces back to one. This forms a system response curve. The area between the curve and the normal performance line ($Q(t) = 1$) forms a triangle, the area of which, effectively, is the cumulative loss of service

and indicates how resilient the system is (see Figure 5). For a given day, 250 failure scenarios are sampled. Therefore, each failure scenario corresponds to a resilience curve and a LOS. The distribution of the 250 LOS shows the likelihood of the outcomes (loss of service) and indicates the system's resilience. A high LOS value means a high degree of service loss overall and is therefore associated with low resilience.
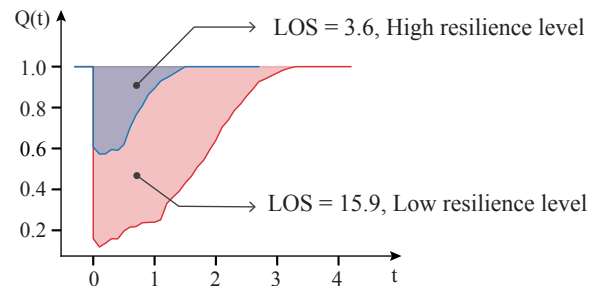

Fig. 5: Resilience curve with calculated LOS

A time series of annual total LOS is constructed using the simulation results of the example days and the clustering analyses. This is done by duplicating the simulation results for each example day and assigning them to all days in the same cluster. The days are then grouped by year and the convolution of all non-zero distributions is computed to give the estimation of the annual total LOS. From Figure 6, the constructed time series data shows an overall upward trend regarding the estimated annual total LOS. Moreover, the spikes suggest that, in the climate model output used, there exist some extremely hot years with significantly more and hotter days. The overall upward trend suggests that the railway system's resilience to high-temperature-induced disruptions could be compromised under future climate scenarios.
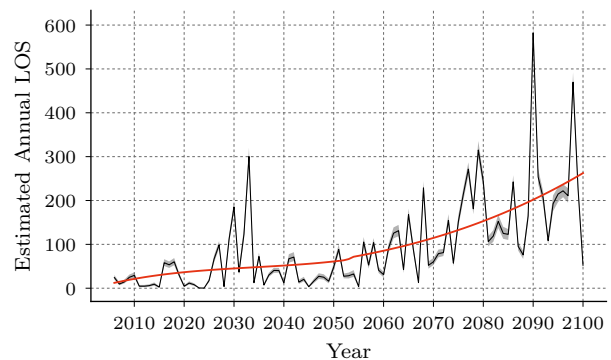
Fig. 6: Time series of the estimated annual total LOS for the 2006-2100 period. The solid black line shows the expectations of the aggregated distributions. The shaded area shows the 5% to 95% range across the aggregated distribution. The solid red line is obtained by smoothing the solid black line with a Savitzky–Golay filter [54].

D. Shock-disruption relationship

In this case study, the external weather condition is regarded as a form of external shock imposed on the railway system.

Fig. 7: The relationship between: (a) The average of measured cumulative loss of service, $\mathcal{LOS}$ and the national average tasmax; (b) the expectation of the number of edge removed Ψ and the national average tasmax; (c) The average of measured cumulative loss of service, $\mathcal{LOS}$ a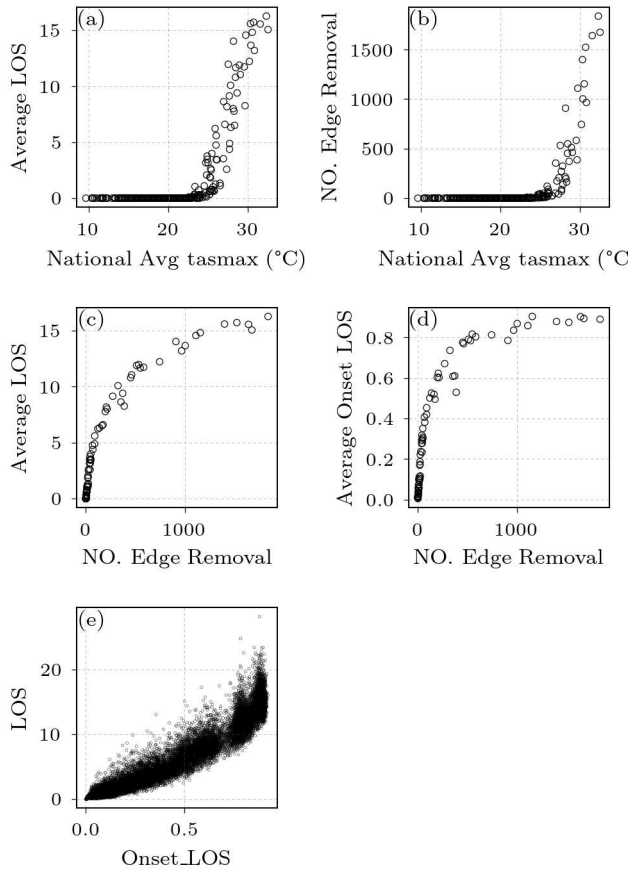nd expectation of the number of edge removal, Ψ; (d) the expectation of the number of edge removed Ψ and the average of loss of service, $\mathcal{LOS}$ at the onset of disruption; (e) the average of cumulative loss of service, $\mathcal{LOS}$ and the onset loss of service. The national average tasmax is the average of the tasmax across the asset layer.

The direct effect of such shock is the failure and removal of edges from the asset layer. Service disruption occurs when the railway system fails to deliver part of its service. Infrastructure systems are believed to be complex systems that often exhibit non-linearity. The railway system in this case study is no exception, as a non-linear relationship is observed between the intensity of external shock received and the severity of service disruption caused.

Figure 7a shows this shock-disruption relation, with the intensity of the shock measured by the national average of tasmax and the severity of the disruption indicated by the simulated LOS. The plot uses the simulation results of the 84 example days, whose expected number of failure, Ψ, is greater than 1. For each day, the national average of tasmax is plotted against the simulated cumulative loss of service. As the temperature increases, the increase of the consequential loss of services presents a threshold behavior with an apparent surge as the temperature increase above 25 °C. Following the surge, there is a steady increase with the increasing temperature, which then shows a trend to plateau. This suggests the possibility that changes in the climate system can lead to some disproportional disruptions to the infrastructure systems.

This shock-disruption relationship is then further broken down into a shock-damage-disruption relation. The shock-disruption relationship in Figure 7a is, in fact, a combined effect of the shock-damage relationship in Figure 7b and the damage-disruption relationship in Figure 7c. Figure 7b shows the relationship between the intensity of the shock and the extent of damage caused, where a surge happens at a 25 °C national average of tasmax followed by a steady increase with increasing temperature. Figure 7c shows the relationship between the extent of damage caused and the severity of service disruption. The plot has a sharp increase as few edges are removed and then keeps on growing at a slower rate. The damage-disruption relation in Figure 7c is then broken down in Figure 7d and Figure 7e. Figure 7d shows the relationship between the number of edges removed and the scale of disruption caused at the onset of the event. Figure 7e shows the relationship between the onset service disruption (without any rerouting or repairing) and the cumulative loss of service. The plots suggest that the non-linear relationship between the number of edge removal and the onset of service disruption is one of the main contributors to the overall observed system non-linearity.

E. Climate-based, random and targeted failures

As mentioned in Section I, neither the random failure scenarios, where failures happen randomly across the network, nor the targeted attack strategy, where network component failures are targeted to simulate the most extensive possible disruption, may be able to capture the feature of weather-related disruptions. Therefore, two separate sets of simulations, one implementing the random failure scenarios and the other implementing the targeted attack strategy, are carried out to compare the effects of these against climate-based disruption. For a given day, the expected number of edge failures, Ψ, is calculated using Equation 8. Then, for the random strategy, in each Monte Carlo run, Ψ number of edges are randomly selected and removed from the network, followed by the same rerouting and repairing efforts with LOS calculated using the same approach. For the targeted strategy, the first Ψ edges with the most traffic are removed from the network, followed by the same assessment procedure.

Firstly, the percentages of OD flows interrupted at the onset of component failure without any rerouting or repair attempts are compared between the three strategies (Figure 8). When the same number of edges are removed from the network, the strategy that results in a higher percentage of OD disruption is believed to be more disruptive. The results show that climate-based strategy tends to sit between random and targeted. In particular, for the extent of the failed portion of the network edges intermediate between a sparse and a total number of failures, the climate-based strategy is more

disruptive than random and less disruptive than targeted. For an extremely high number of edges involved, the disruption of a random strategy would exceed the one generated by the climate-based though there is only a slight difference between the three strategies. The Mann-Whitney U test [55] is carried out between samples from the climatic-based and random failure scenarios. This specific test was chosen because more than half (45 out of 84 for the climate-based scenarios, and 61 out of 84 for the random scenarios) of the sampled LOS fails the normality test with a significance level of 0.01. The null hypothesis for the Mann-Whitney U test is that the distributions of the two samples are identical and the alternative hypothesis is that they are not identical. With a significance level of 0.01, the null hypothesis is rejected in 76 out of the total 84 instances. The results of the statistical tests highlight how different climatic disruptions are from random disruptions.
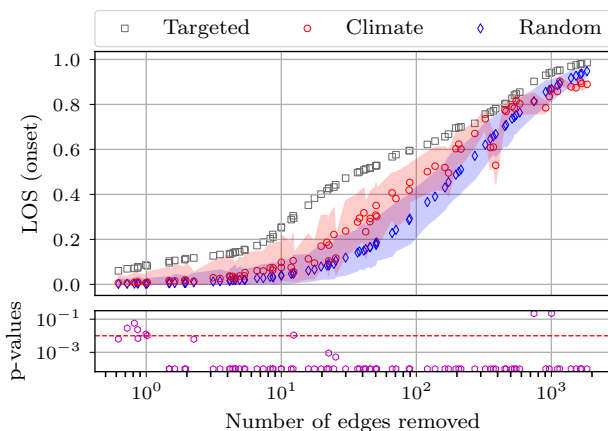

Fig. 8: upper): Percentage of OD journey interrupted at the onset of disruption without any rerouting or repairing effort against the number of nodes removed. The sample size is 250. The shaded area shows the 2.5% to 97.5% range. Markers are the means of each sample. lower): P-value of the Mann-Whitney U test between samples from climatic and random failure scenarios vs. the number of nodes removed. Any p-value smaller than 0.0001 is replaced with 0.0001. The red horizontal line is p=0.01, the confidence level adopted.

Figure 9 shows the distribution of the measured cumulative loss of service against the number of edges removed for the three strategies. Though discernible differences exist between the LOS sampled from the climate-based failure scenarios and the random strategy, the Mann-Whitney U tests are carried out between the samples. This specific test was chosen because the majority (167 out of 168) of the sampled LOS failed the normality test with a significance level of 0.01. The null hypothesis for the Mann-Whitney U test is that the distributions of the two samples are identical and the alternative hypothesis is that they are not identical. With a significance level of 0.01, the null hypothesis is rejected in 74 out of the total 84 instances. It suggests that the LOS sampled from climate-based failure scenarios are statistically different from those sampled with random failure in most cases. In contrast, the targeted

strategy sits distinctly above both the random and the climate-based for all extents of edge failure. Overall, the system suffers a higher level of loss of service under the climate-based failure scenarios than the random one when the same number of edges are removed from the network. It means the system has a higher level of resilience toward random failure scenarios than climate-based ones.
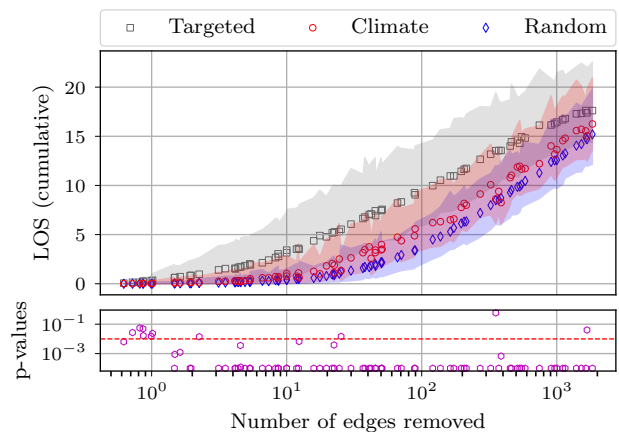

Fig. 9: upper)The measured LOS against the number of edges removed. The sample size is 250. The shaded area shows the 2.5% to 97.5% range. Markers are the means of each sample. lower) P-values of the Mann-Whitney U test between samples from climate-based and random failure scenarios against the number of nodes removed. Any p-value smaller than 0.0001 is replaced with 0.0001 for visualization purposes. The red horizontal line is p=0.01, the confidence level adopted.

IV. DISCUSSION

The case study points to three key findings. 1) There is an overall increasing trend in the estimated annual total LOS over the 95-year period, where increased frequency and intensity of extreme events drive the average LOS upwards. 2) The severity of the disruptions caused, measured with the cumulative LOS, increases non-linearly with the increasing intensity of the external shock applied. This non-linearity is a combined effect of the threshold behavior between the national average temperature and the number of edges removed (Figure 7b) and the nonlinear relationship between the number of edges removed and average onset disruption (Figure 7d). The reason behind the nonlinear relationship between the number of edges removed and average onset disruption is down to the nature of complex systems, where the behavior or response of the system is distinct from the combined behavior or response of its components [19]. The key message here is that climate change impact assessment should not stop at the assessment of asset-level physical damage but need to be taken to system-level functional loss.

3) Random failure models tend to overestimate the network's resilience compared to climate-based failure scenarios. When climate-based disruptions are considered, the network function degradation is more severe than in the random failure scenarios. This finding supports our working hypothesis that

infrastructure systems may behave differently under different failure scenarios and evidence the need to use realistic weather profiles generated by climate models. Further exploration of the reason behind this would require more simulations with various failure scenarios to test any proposed hypothesis and is beyond the scope of this work. The most remarkable difference between the random failure scenario and the climate-based failure scenario is that all assets are of equal probability of failure in the random failure situation whilst, in the climate-based failure scenario, the assets are subjected to unequal probability of failure and assets of close geographical proximity are likely to have similar probabilities of failure. Future works could look at if such spatial correlations of weather-induced failures are leading to clusters of assets within close geographic proximity being affected simultaneously.

We consider these findings from the case study not specific to the infrastructure model and climate model used. Regardless of the specific choices for this case study, the method remains valid as it does not rely on specific features of the dataset chosen. As for the climate dataset, to completely prove the universality of the phenomenon observed, simulations of output from all climate models would be required and is of huge computational cost. The evidence we found about the difference between random and climate-induced failures holds across the vast majority of the days examined. The conditions found in our sample could be found in any dataset where only the distribution of the magnitude and the frequencies change.

The direct use of climate model outputs also provides the possibility to assess the resilience of the infrastructure systems to different climate change scenarios and provides a more comprehensive assessment of the threat of climate change. This is achieved through two aspects. First, the introduction of the Monte Carlo simulation in the assessment framework provides a density distribution of the possible extent of service loss in the future instead of a single numerical value. It provides a sense of how broad the outcomes would fall and the associated likelihood of those outcomes. Second, it can exploit the tremendous number of datasets climate change research provides for future climate projections. One climate model output dataset can only provide one possible view into the future, and only a sufficient collection of outputs from different climate model simulation runs can give a more reliable prediction with the degree of uncertainty and error range addressed.

The proposed approach initiates disruptive events in infrastructure systems using the output data from climate change research. Such an approach offers advances compared to the weather generation methods used in literature [36], [38], [39]. Those methods mostly involve some form of manipulation of present-day weather statistics and presume that future weather patterns remain the same as the current day. The proposed method overcomes such presumptions and can generate behaviorally realistic and physically viable climate hazards under future climate change scenarios. However, the proposed approach is limited by the spatial and temporal resolution of the climate change data. For example, the highest spatial resolution offered by EURO-CORDEX is ∼12km and the majority of the outputs are with a daily temporal resolution. In

contrast, those weather simulators can offer up to half-hourly weather profiles. Although the case study here only requires daily weather profiles, future applications of the method may require weather profiles of higher temporal resolution.

The proposed failure initiation approach is applicable to any infrastructure system with most types of climate hazards, provided the fragility functions become available. By introducing multiple inter-dependent asset layers subjected to multiple climate hazards, the proposed approach has the potential to simulate cascading failures in an interconnected infrastructure network and assess the resilience of the system. Future applications of the approach should see case studies on interdependent infrastructure systems with compound climate hazards.

The case study also highlights challenges and limitations in implementing the proposed approach and points to directions and improvements to consider when conducting further case studies. The Monte Carlo simulation requires substantial amounts of computational power. In the case study, simplifications and assumptions are made to s few aspects of the assessment framework to bring the amount of calculation within the computational power available and to keep the emphasis on improving the representativeness of the spatial pattern of climate hazards.

A clustering analysis was carried out to select representative example days (representative spatial patterns of the hazard). Doing so brings the amount of calculation within computational power available and provides important insights into the 95-year trend. A single day is assumed as an independent weather event in the case study and considered as an instance of situations the railway system might face. This assumption holds because, in real-world practice, repair work will not be carried out until the heatwave is passed [53]. For future works on quantifying the impact of increasing frequency and intensity of heatwaves, one can use more advanced machine learning techniques to identify representative heatwaves.

Spatial patterns and temporal patterns are two major aspects of recreating weather events and climate hazards in infrastructure resilience assessment frameworks. We understand that both aspects of climate hazards are of equal importance and interest. With limited computational memory, this work focuses on improving the resolution of the spatial features of climate hazards and uses detailed daily weather profiles with realistic geographical variations. Moving forward, efforts can be put into integrating time series analysis into the current assessment framework.

The second challenge is the lack of empirical data and information on industrial practice for the specification of fragility functions and railway system dynamics. For example, the industrial practice of rerouting, the prioritization of repairing, and the estimation of spare capacity. A few assumptions are made in the case study to the most general form to complete the resilience assessment setup in the absence of sufficient information. In the case study, all track segments are assumed to have the same fragile function with the same critical temperature. In reality, the Critical Rail Temperature (CRT) varies from track to track and depends on many factors including the stress-free temperature of the rail, the

quality and degree of consolidation of the ballast, ballast shoulders, tamping, the type and condition of the sleepers and fastenings, and maintenance and renewal work [49]. Provided such information becomes available, which informs asset-specific fragility functions, more rigorous quantification of infrastructure resilience to future climate can be addressed.

Advancements can be made to the recovery processes. The probability of repair at the moment is kept at a 50% chance for all damaged assets. Future works can introduce a 'cap' to limit the number of assets that can be repaired at a given time step to reflect the limited resources to perform system repair. Or express the probability of recovery as a function of multiple factors, such as the geographical proximity to repairing resource centers and the next day's weather conditions. If the probability of recovery is set to be associated with network topological metrics, e.g., betweenness centrality, different network recovery strategies can be tested with the proposed framework.

V. Conclusion

This work presented a method to generate network failure scenarios and system disruptions using climate change research data for the assessment of the infrastructure system's climate resilience. The case study attempts to quantify the resilience of Great Britain's railway passenger transport system to high-temperature-related track buckling under the RCP8.5 climate change scenario. Findings from the case study support the two arguments that motivate this framework's proposal: 1) Random failure models tend to overestimate the network's resilience; 2) The system quality of services degrades nonlinearly with the magnitude of the disruption. Together, they prove the need for linking climate change resilience assessment to system-level functional loss as opposed to a mere count of the failed nodes or the identification of a threshold for network fragmentation.

References

[1] S. Rinaldi, J. Peerenboom, and T. Kelly, "Identifying, understanding, and analyzing critical infrastructure interdependencies," IEEE Control Systems Magazine, vol. 21, no. 6, pp. 11–25, 2001.

[2] M. Chester, B. S. Underwood, B. Allenby, M. Garcia, C. Samaras, S. Markolf, K. Sanders, B. Preston, and T. R. Miller, "Infrastructure resilience to navigate increasingly uncertain and complex conditions in the anthropocene," npj Urban Sustainability, vol. 1, no. 1, p. 4, 2021. [Online]. Available: https://doi.org/10.1038/s42949-021-00016-y

[3] E. J. Palin, I. Stipanovic Oslakovic, K. Gavin, and A. Quinn, "Implications of climate change for railway infrastructure," Wiley Interdisciplinary Reviews: Climate Change, vol. 12, no. 5, p. e728, 2021.

[4] J. K. Hillier and R. S. Dixon, "Seasonal impact-based mapping of compound hazards," Environmental Research Letters, vol. 15, no. 11, p. 114013, 2020.

[5] T. W. Corringham, J. McCarthy, T. Shulgina, A. Gershunov, D. R. Cayan, and F. M. Ralph, "Climate change contributions to future atmospheric river flood damages in the western united states," Scientific reports, vol. 12, no. 1, pp. 1–9, 2022.

[6] IPCC, Climate Change 2013: The Physical Science Basis. Contribution of Working Group I to the Fifth Assessment Report of the Intergovernmental Panel on Climate Change. Cambridge, United Kingdom and New York, NY, USA: Cambridge University Press, 2013. [Online]. Available: www.climatechange2013.org

[7] S. S.I., X. Zhang, M. Adnan, W. Badi, C. Dereczynski, A. Di Luca, S. Ghosh, I. Iskandar, J. Kossin, S. Lewis, F. Otto, I. Pinto, M. Satoh, S. M. Vicente-Serrano, M. Wehner, and B. Zhou, "Weather and climate extreme events in a changing climate," in Climate Change 2021: The Physical Science Basis. Cambridge University Press, 2021.

[8] EU-CIRCLE, "EU-CIRCLE: D3.2 report on climate related critical event parameters." [Online]. Available: https://www.eu-circle.eu/wp-content/uploads/2018/10/D3.2.pdf

[9] M. Office, "2019: A year in review," Dec 2019, https://www.metoffice.gov.uk/about-us/press-office/news/weather-and-climate/2019/weather-overview-2019, accessed 27.02.2022.

[10] J. Finlay and P. Bolton, "Autumn and winter floods, 2019-20." [Online]. Available: https://commonslibrary.parliament.uk/research-briefings/cbp-8803/

[11] M. Kendon, "Unprecedented extreme heatwave, july 2022," 2022, https://www.metoffice.gov.uk/about-us/press-office/news/weather-and-climate/2022/july-heat-climate.

[12] R. Betts, A. Haward, and K. Pearson, "The third uk climate change risk assessment," Prepared for the Climate Change Committee, London, 2021.

[13] P. Bubeck, L. Dillenardt, L. Alfieri, L. Feyen, A. H. Thieken, and P. Kellermann, "Global warming to increase flood risk on european railways," Climatic Change, vol. 155, no. 1, pp. 19–36, 2019.

[14] E. E. Koks, J. Rozenberg, C. Zorn, M. Tariverdi, M. Vousdoukas, S. A. Fraser, J. Hall, and S. Hallegatte, "A global multi-hazard risk analysis of road and railway infrastructure assets," Nature communications, vol. 10, no. 1, p. 2677, 2019.

[15] I. V. Sanchis, R. I. Franco, P. M. Fernández, P. S. Zuriaga, and J. B. F. Torres, "Risk of increasing temperature due to climate change on high-speed rail network in spain," Transportation Research Part D: Transport and Environment, vol. 82, p. 102312, 2020.

[16] EU-CIRCLE, "EU-CIRCLE: D3.5 holistic CI climate hazard risk assessment framework." [Online]. Available: https://www.eu-circle.eu/wp-content/uploads/2018/10/D3.5.pdf

[17] A. Mostafavi, "A system-of-systems framework for exploratory analysis of climate change impacts on civil infrastructure resilience," Sustainable and Resilient Infrastructure, vol. 3, no. 4, pp. 175–192, 2018.

[18] S. Wilkinson, S. Dunn, R. Adams, N. Kirchner-Bossi, H. J. Fowler, S. G. Otálora, D. Pritchard, J. Mendes, E. J. Palin, and S. C. Chan, "Consequence forecasting: A rational framework for predicting the consequences of approaching storms," Climate Risk Management, vol. 35, p. 100412, 2022.

[19] G. Punzo, R. Beasley, G. Clarke, N. Holt, S. Jobbins, and M. Mayfield, "Challenges of complexity and resilience in complex engineering systems," ENCORE Network+ White Paper.

[20] J. Lin and Y. Ban, "Complex network topology of transportation systems," Transport reviews, vol. 33, no. 6, pp. 658–685, 2013.

[21] C. Robson, S. Barr, A. Ford, and P. James, "The structure and behaviour of hierarchical infrastructure networks," Applied Network Science, vol. 6, no. 1, pp. 1–25, 2021.

[22] E. J. Hearnshaw and M. M. Wilson, "A complex network approach to supply chain network theory," International Journal of Operations & Production Management, vol. 33, no. 4, pp. 442–469, 2013.

[23] R. Pant, J. W. Hall, and S. P. Blainey, "Vulnerability assessment framework for interdependent critical infrastructures: case-study for great britain's rail network," European Journal of Transportation and Infrastructure Research, vol. 16, no. 1, pp. 174–194, 2016.

[24] N. Goldbeck, P. Angeloudis, and W. Y. Ochieng, "Resilience assessment for interdependent urban infrastructure systems using dynamic network flow models," Reliability Engineering & System Safety, vol. 188, pp. 62–79, 2019.

[25] N. Sharma and P. Gardoni, "Mathematical modeling of interdependent infrastructure: An object-oriented approach for generalized network-system analysis," Reliability Engineering & System Safety, vol. 217, p. 108042, 2022.

[26] X. Liu, D. Li, M. Ma, B. K. Szymanski, H. E. Stanley, and J. Gao, "Network resilience," Physics Reports, vol. 971, pp. 1–108, 2022.

[27] R. Albert, H. Jeong, and A.-L. Barabási, "Error and attack tolerance of complex networks," Letters to Nature, vol. 406, no. 1-3, pp. 378–382, 2000.

[28] G. Dong, Y. Luo, Y. Liu, F. Wang, H. Qin, and A. L. Vilela, "Percolation behaviors of a network of networks under intentional attack with limited information," Chaos, Solitons & Fractals, vol. 159, p. 112147, 2022.

[29] J. Elsner and A. Tsonis, "Nonlinear prediction, chaos, and noise," Bulletin of the American Meteorological Society, 1992.

[30] B. Berche, C. Von Ferber, T. Holovatch, and Y. Holovatch, "Resilience of public transport networks against attacks," The European Physical Journal B, vol. 71, no. 1, pp. 125–137, 2009.

[31] M. Bessani, J. A. Massignan, R. Z. Fanucchi, M. H. Camillo, J. B. London, A. C. Delbem, and C. D. Maciel, "Probabilistic assessment of power distribution systems resilience under extreme weather," IEEE Systems Journal, vol. 13, no. 2, pp. 1747–1756, 2018.

[32] A. N. Tari, M. S. Sepasian, and M. T. Kenari, "Resilience assessment and improvement of distribution networks against extreme weather events," International Journal of Electrical Power & Energy Systems, vol. 125, p. 106414, 2021.

[33] A. Younesi, H. Shayeghi, A. Safari, and P. Siano, "A quantitative resilience measure framework for power systems against wide-area extreme events," IEEE Systems Journal, vol. 15, no. 1, pp. 915–922, 2020.

[34] D. N. Trakas, M. Panteli, N. D. Hatziargyriou, and P. Mancarella, "Spatial risk analysis of power systems resilience during extreme events," Risk Analysis, vol. 39, no. 1, pp. 195–211, 2019.

[35] H. Sabouhi, A. Doroudi, M. Fotuhi-Firuzabad, and M. Bashiri, "Electrical power system resilience assessment: A comprehensive approach," IEEE Systems Journal, vol. 14, no. 2, pp. 2643–2652, 2019.

[36] M. Panteli and P. Mancarella, "Influence of extreme weather and climate change on the resilience of power systems: Impacts and possible mitigation strategies," Electric Power Systems Research, vol. 127, pp. 259–270, 2015.

[37] ——, "Modeling and evaluating the resilience of critical electrical power infrastructure to extreme weather events," IEEE Systems Journal, vol. 11, no. 3, pp. 1733–1742, 2015.

[38] M. Panteli, C. Pickering, S. Wilkinson, R. Dawson, and P. Mancarella, "Power system resilience to extreme weather: fragility modeling, probabilistic impact assessment, and adaptation measures," IEEE Transactions on Power Systems, vol. 32, no. 5, pp. 3747–3757, 2016.

[39] G. Fu, S. Wilkinson, R. J. Dawson, H. J. Fowler, C. Kilsby, M. Panteli, and P. Mancarella, "Integrated approach to assess the resilience of future electricity infrastructure networks to climate hazards," IEEE Systems Journal, vol. 12, no. 4, pp. 3169–3180, 2018.

[40] N. Bhusal, M. Gautam, M. Abdelmalak, and M. Benidris, "Modeling of natural disasters and extreme events for power system resilience enhancement and evaluation methods," in 2020 International Conference on Probabilistic Methods Applied to Power Systems (PMAPS). IEEE, 2020, pp. 1–6.

[41] "Earth system grid federation," https://esgf.llnl.gov/index.html, (accessed: 28.02.2022).

[42] P. Camus, A. Tomás, G. Díaz-Hernández, B. Rodríguez, C. Izaguirre, and I. Losada, "Probabilistic assessment of port operation downtimes under climate change," Coastal Engineering, vol. 147, pp. 12–24, 2019.

[43] NIC, "Anticipate, react, recover. resilient infrastructure systems," National Infrastructure Commission, 2020.

[44] A. R. Berkeley, M. Wallace, and C. Coo, "A framework for establishing critical infrastructure resilience goals," Final report and recommendations by the council, national infrastructure advisory council, pp. 18–21, 2010.

[45] M. Bruneau, S. E. Chang, R. T. Eguchi, G. C. Lee, T. D. O'Rourke, A. M. Reinhorn, M. Shinozuka, K. Tierney, W. A. Wallace, and D. Von Winterfeldt, "A framework to quantitatively assess and enhance the seismic resilience of communities," Earthquake spectra, vol. 19, no. 4, pp. 733–752, 2003.

[46] F. Pedregosa, G. Varoquaux, A. Gramfort, V. Michel, B. Thirion, O. Grisel, M. Blondel, P. Prettenhofer, R. Weiss, V. Dubourg, J. Vanderplas, A. Passos, D. Cournapeau, M. Brucher, M. Perrot, and E. Duchesnay, "Scikit-learn: Machine learning in Python," pp. 2825–2830, 2011.

[47] E. J. Palin, H. E. Thornton, C. T. Mathison, R. E. McCarthy, R. T. Clark, and J. Dora, "Future projections of temperature-related climate change impacts on the railway network of great britain," Climatic Change, vol. 120, no. 1, pp. 71–93, 2013.

[48] E. Ferranti, L. Chapman, C. Lowe, S. McCulloch, D. Jaroszweski, and A. Quinn, "Heat-related failures on southeast england's railway network: Insights and implications for heat risk management," Weather, Climate, and Society, vol. 8, no. 2, pp. 177–191, 2016.

[49] Network-Rail, "Nr/l3/trk/7012: Critical rail temperature management for projects."

[50] A. Vajda, H. Tuomenvirta, I. Juga, P. Nurmi, P. Jokinen, and J. Rauhala, "Severe weather affecting european transport systems: the identification, classification and frequencies of events," Natural Hazards, vol. 72, no. 1, pp. 169–188, 2014.

[51] V. Ramdas and D. Chapman, "Project report cpr2282: Options for capacity measures/metrics," 2017, https://www.orr.gov.uk/sites/default/files/om/trl_report_options_for_capacity_measures_and_metrics.pdf.

[52] J. Edmonds and R. M. Karp, "Theoretical improvements in algorithmic efficiency for network flow problems," Journal of the ACM (JACM), vol. 19, no. 2, pp. 248–264, 1972.

[53] Network-Rail, "Nr/l2/trk/3011: Continuously welded rail (cwr) track."

[54] [Online]. Available: https://docs.scipy.org/doc/scipy/reference/generated/scipy.signal.savgol_filter.html

[55] H. B. Mann and D. R. Whitney, "On a Test of Whether one of Two Random Variables is Stochastically Larger than the Other," The Annals of Mathematical Statistics, vol. 18, no. 1, pp. 50 – 60, 1947. [Online]. Available: https://doi.org/10.1214/aoms/1177730491

Qianqian Li received the M.Eng. degree in Architectural Engineering from the University of Sheffield, Sheffield, U.K. in 2019. She is currently pursuing the Ph.D. degree in civil engineering with the resource, infrastructure systems, built-environments (rise) group at the University of Sheffield. Her research interest is in complex networks and their application to infrastructure systems. Her Ph.D. focuses on analyzing the resilience of infrastructure systems to climate change.

Giuliano Punzo graduated in aerospace engineering and briefly joined industry before his Ph.D. at the University of Strathclyde. Dr Punzo's interests span robotics, control theory, consensus and complexity. Dr Punzo joined the department of Automatic Controls and Systems Engineering at the University of Sheffield as a Lecturer in 2019, after post-doctoral appointments at the University of Glasgow, the University of Strathclyde and at the University of Sheffield.

Craig Robson is a lecturer in the School of Engineering, Newcastle University, focused on spatial data science. His research interests include complex networks, infrastructure network resilience, spatial data management, and data visualization. Craig was awarded a PhD in 2017 from Newcastle University on the resilience of hierarchical infrastructure networks, before a post-doc position on infrastructure resilience and integrated assessment platforms for critical infrastructure modeling.

Hadi Arbabi received their M.Eng. degree in Architectural Engineering and Ph.D. degree from the University of Sheffield in 2015 and 2019. Hadi is currently a lecturer in the Department of Civil & Structural Engineering at the University of Sheffield. Hadi's work and research interests sit at the interface of data-driven urban analytics and planning. Their overall body of research focuses on the challenges relating to resource consumption and productivity in urban systems often in the context of climate change.

Martin Mayfield is a Professor of Engineering Design at the University of Sheffield. His expertise spans a diverse array of systems engineering, sustainable design, climate change mitigation and adaptation, mission-critical systems, city systems, and mapping infrastructure interdependencies. He recognizes the opportunities presented by Complexity Science to improve the resilience and performance of complex adaptive systems such as future energy systems, cities, and our national infrastructure.

Supplementary Material

The modified minimum-cost maximum-flow algorithm based on the Edmonds-Karp algorithm [1] used for the rerouting in the case study is described in ALGORITHM 1.

Any edge, if undamaged, is assumed to have a spare capacity of 50%[1] of its regular traffic for the rerouting. At each time step, the algorithm implements 5 rounds of path searching. At each round of path searching, it searches for the shortest path that, 1) all edges forming the path has available spare capacity; and 2) is within twice[1] the geographical length of the original path for each disrupted OD pair. The available capacity of the path is the smallest spare capacity across all the edges forming the path. Any used spare capacity is deduced before the next round of path searching. The capacity is gradually used and in some cases, the capacities of some popular edges are reduced to 0 in the first round of path searching.

The code involves a large amount of path search as there are 2,282,270 OD pairs in the system model with an asset layer constituting 2484 nodes and 4524 edges. The search for alternative paths is time-consuming and memory-intensive. To meet the limitation in computational power available, the algorithm is set to eliminate the alternative path search for any OD pair with fewer than 15 passenger trips or geographical path length less than 30km. Those trips can be regarded as trips that are likely to be aborted due to their relatively small demand figures or met by using alternative transportation services due to their short geographical distance. These include OD pairs with potentially no passengers in the days considered, which, together, contribute to 99% toward OD pair count. By eliminating those OD pairs from the path search, the

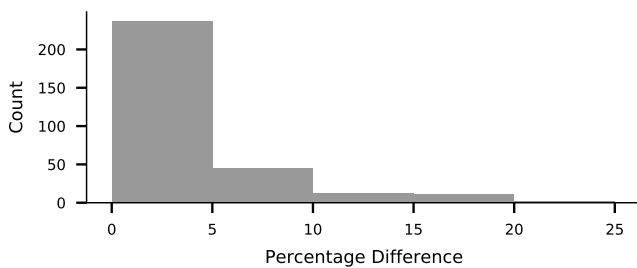[1]This is an arbitrary value set on the absence of relevant information.

Fig. 1: Histogram of the percentage difference between the amount of flow delivered at each time step between a full rerouting effort and the reduced rerouting effort. Twelve failure scenarios are included in the sample. The number of trips delivered with the two rerouting efforts is compared at every time step.

computational time can be reduced by 96%. In fact, the sum of those OD pairs contributes 71% toward total passenger trips. The non-rerouted demand is assumed to resume travel as the service is re-established on the original path. Up to that time, it counts as unsatisfied demand. A small-scale trial computation was carried out to assess the suitability of this approach. The difference in the absolute amount of flow delivered between a full rerouting and the reduced rerouting strategy chosen is less than 5% in the vast majority of the cases (Figure 1).

ALGORITHM 1 - The Rerouting Algorithm

INPUT:
- R - residual functioning network structure.
- $\mathbf{c}_{u,v}$, - edge capacity
- $\mathbf{D}^{re}$ - OD flows to be rerouted.

$count = 0$

WHILE $count <$ Nr of path search:
- For all OD pairs that $D^{re}_{od} > 0$:
  - If there is no path...OK
  - If there is a path, P_{od}:
    - if path length $< 2 \times$ the original path length, DO:
      - temporarily allocated flow $T'^{re}_{od} = \min(c_{u,v}, \ (u,v) \in P_{od})$
      - for all edges in the path: $f^r_{u,v} += T'^{re}_{od}$
- For edge (u,v) in R:
  - If $f^r_{u,v} > c_{u,v}$:
    - reduction factor, $\varphi_{u,v} = c_{u,v}/f^r_{u,v}$
    - $c_{u,v} = 0$
  - Else $f^r_{u,v} \le c_{u,v}$:
    - reduction factor, $\varphi_{u,v} = 1$
    - $c_{u,v} -= f^r_{u,v}$
- For (o,d) in $\mathbf{D}^{re}$:
  - $\varphi_{od} = \min(\varphi_{u,v}, \ (u,v) \in P_{od})$
  - $T^{re}_{od} += T'^{re}_{od} * \varphi_{od}$
  - $D^{re}_{od} -= T'^{re}_{od} * \varphi_{od}$
- Remove edges that $c_{u,v} = 0$ from R
- $count += 1$

RETURN T^{re} - Trips delivered through rerouting

REFERENCES

[1] J. Edmonds and R. M. Karp, "Theoretical improvements in algorithmic efficiency for network flow problems," Journal of the ACM (JACM), vol. 19, no. 2, pp. 248–264, 1972.